Available online at www.sciencedirect.com
ScienceDirect
Catalysis Today 125 (2007) 248–255
CATALYSIS TODAY
www.elsevier.com/locate/cattod

Hydrodenitrogenation of carbazole over a series of bulk Ni_xMoP catalysts

Ibrahim I. Abu, Kevin J. Smith *

Department of Chemical & Biological Engineering, University of British Columbia, 2360 EastMall, Vancouver, BC, Canada V6T 1Z3

Available online 10 April 2007

Abstract

The hydrodenitrogenation (HDN) of carbazole over bulk Ni_xMoP ($0 \leq x \leq 1.1$) catalysts is reported at 583 K and 3.0 MPa H_2. X-ray diffraction (XRD) revealed the presence of NiMoP and MoP in the Ni_xMoP catalysts. The Ni_xMoP had higher CO uptake, higher acidity and lower TOFs for the HDN of carbazole than MoP. However, the selectivity to bicylohexane (BCHX) was greater on the Ni_xMoP catalysts compared to MoP, and the $Ni_{0.07}MoP$ had the highest BCHX selectivity and highest TOF among the Ni_xMoP catalysts. The improved selectivity is attributed to the enhanced CO uptake and acidity that resulted in increased hydrogenation of carbazole to terahydrocarbazole which in turn readily undergoes C–N bond cleavage on acid sites to produce BCHX.

Keywords: Hydrodenitrogenation; Metal phosphide; Catalyst; MoP; NiMoP; Carbazole

1. Introduction

Hydrotreating is an important crude oil refining process that removes S, N and O from hydrocarbon molecules by reacting them with H_2 over a catalyst. Improving the activity of hydrodenitrogenation (HDN) and hydrodesulfurization (HDS) catalysts, by addition of phosphorous to conventional Co–Mo, Ni–Mo and Ni–W sulfides [1–15], and by the development of new catalysts such as metal carbides, metal nitrides [16–20] and more recently metal phosphides [21–27], has been described in the literature. In some studies metal phosphides have been shown to be more active than conventional metal sulfides for HDS [28,29] and HDN [25,30]. The transition metal monophosphides (M/P = 1) and metal-rich phosphides (M/P > 1) are of most interest in hydrotreating catalysis because of their superior stability compared to phosphorous rich (M/P < 1) metal phosphides [21]. Both bulk and supported metal phosphides can be prepared by the temperature-programmed-reduction (TPR) of the corresponding metal phosphates [26–34].

The mechanism of HDN of N-containing heterocycles is well known on sulfided catalysts [35–37]. The first step of the reaction is the hydrogenation of the aromatic ring to which the amino group is attached, followed by C–N bond scission. Once hydrogenated, the C–N bond cleavage is accomplished through elimination or nucleophilic substitution. During such Hoffman elimination reactions, the N atom is quarternized by an acid, creating a better leaving group, and the presence of a base removes the β-hydrogen atom. An important condition for enhancing the reaction in this mechanism is the presence of H_2S and the formation of carbenium ions or carbanions. Oyama [27] has pointed out, however, that on phosphides the most likely HDN pathway is the initial activation of the heterocycle at the α-position after which the N-containing ring undergoes further reaction involving the elimination of the β-hydrogen atom. In either case, the catalyst acidity and hydrogenation capability plays an important role in determining the overall catalyst activity and selectivity, and these functions are in turn determined by the catalyst composition.

The activity of Co_2P, Ni_2P, CoP, WP as well as NiMoP and CoMoP for the HDN of *ortho*-propylaniline has been described in the literature [31]. In addition, the HDN and HDS activity of the metal phosphides has been compared with that of conventional metal sulfide catalysts using feeds of S- and N-containing heterocycles [24,27,29]. The effect of composition of supported $Ni_{2x}Mo_{(1-x)}P$ catalysts on the HDN of *ortho*-propylaniline in the presence and absence of H_2S has also been

* Corresponding author. Tel.: +1 604 822 3601; fax: +1 604 822 6003.
E-mail address: kjs@interchange.ubc.ca (K.J. Smith).

0920-5861/$ – see front matter
doi:10.1016/j.cattod.2007.02.035

reported in the literature [38] with the catalyst composition in the range P (0–4 wt%), Ni (0–3 wt%) and Mo (0–12 wt%). The authors reported that MoP/Al_2O_3 produced the highest conversion and selectivity for hydrogenolysis and that incorporating Ni to MoP/Al_2O_3 decreased the hydrogenolysis activity but increased the hydrogenation activity of the catalyst. The formation of NiMoP solid solutions occurs over a wide range of compositions of the $Ni_{(2-x)}Mo_xP$ catalysts [39]. Maity et al. [40] reported that excess phosphorous caused a decrease in the specific area of the NiMoP catalyst, thereby decreasing the catalyst activity and being in agreement with the observation that metal-rich phosphides are more active than phosphorous-rich phosphides. Stinner et al. [25] also reported that MoP has the highest intrinsic activity for HDN of *ortho*-propylaniline among a series of metal phosphide catalysts including NiMoP and CoMoP. The phosphides showed selectivities similar to a conventional MoS_2 catalyst, and in all cases, selectivity to the direct hydrogenolysis product propylbenzene was low.

In the present study we report on the activity of a series of Ni_xMoP ($0.0 \leq x \leq 1.11$) catalysts for the HDN of carbazole. Carbazole is a non-basic refractory heterocycle that has not been used previously to examine the activity of metal phosphide catalysts. In preparing the catalysts, different amounts of Ni were added to the MoP such that the Mo and P content was fixed. Consequently, we obtained metal-rich phosphides that would be expected to have high activity and stability [27]. Furthermore, because of recent results on a series of Co_xNi_2P and Co_xMoP catalysts, in which the P content, catalyst acidity and hence selectivity during HDS of 4,6-dimethyldibenzothiophene were shown to be dependent upon the Co content [41], the present study was aimed at determining if a similar effect was observed with Ni_xMoP catalysts for the HDN of carbazole.

2. Experimental

2.1. Catalyst preparation

All the catalysts were prepared by TPR of the corresponding metal phosphates. Stoichiometric amounts (Mo/P = 1) of ammonium heptamolybdate ($(NH_4)_6Mo_7O_{24}{\cdot}4H_2O$) and diammonium hydrogen phosphate ($(NH_4)_2HPO_4$) were dissolved in a beaker containing 15 ml of de-ionized water. The resulting mixture was stirred at room temperature while adding 10 ml of nickel nitrate solution prepared by dissolving an appropriate amount of nickel hexahydrate ($Ni(NO_3)_2{\cdot}6H_2O$) in 10 ml of deionized water to give the desired mol% Ni in the final Ni_xMoP catalyst. After addition of the Ni solution, the mixture was stirred while evaporating to dryness. The resulting solid was further dried in an oven at 373 K for 2 h and calcined at 773 K for 6 h. The calcined product (or Ni_xMoP precursor) was ground to a powder ($d_P < 0.7$ mm) and subjected to TPR in H_2 (Praxair, 99.99%) at a flow rate of 120 ml (STP)/min and a temperature ramp rate of 1 K/min to a final temperature of 1000 K. The final temperature was held for a period of 2 h. After the reduction, the catalyst was cooled to room temperature in He at a flow rate of 20 ml/min. Prior to removal from the reactor, the Ni_xMoP was passivated in 2 vol.% O_2/He for 2 h at room temperature.

2.2. Catalyst characterization

TPR of the catalyst precursors was conducted in a 60 ml/min flow of 10 vol.% H_2 in Ar using 0.2–0.4 g of the calcined sample loaded into a stainless steel reactor (i.d. = 9 mm). A thermal conductivity detector (TCD) was used to measure the H_2 consumption as the reactor was heated at 1 K/min to the final temperature of 1200 K. The reactor was held at this temperature for 2 h before cooling to 313 K at a rate of 5 K/min. The TCD response was calibrated by reducing a known amount Cu_2O under the same conditions.

Powder X-ray diffraction (XRD) analysis was performed on the passivated catalysts using a Siemens D500 Cu Kα X-ray source of wavelength 1.54 Å. The analysis was performed at 40 kV, a scan range of 3–70° with a step size of 0.04° and step time of 2 s. The phase identification was carried out after subtraction of the background using standard software. Crystallite size (d_c) estimates were made using the Scherrer equation, $d_c = K\lambda/\beta \cos\theta$ where the constant K was taken to be 0.9, λ is the wavelength of radiation, β the peak width in radians and θ is the angle of diffraction.

A single-point BET surface area measurement of the catalysts was made using a Micrometrics FlowSorbII 2300. About 1 g of passivated catalyst was degassed at 393 K for 2 h and the measurement was made using 70 vol.% He/N_2.

A Leybold Max200 X-ray photoelectron spectrometer was used for X-ray photoelectron spectroscopy (XPS) studies. Al Kα was used as the photon source for all the metal phosphides. The Al Kα was generated at 15 kV and 20 mA. The pass energy for the survey scan was set at 192 eV and for the narrow scan it was 48 eV. All catalyst samples were analyzed after passivation at room temperature. Exposure of the samples to ambient atmosphere was minimized by transferring the samples either in vacuum or under nitrogen (UHP). All XPS spectra were corrected to the C 1s peak at 285.0 eV.

The CO uptake was measured using pulsed chemisorption. About 0.5–1.0 g of catalyst was pre-treated in a stainless steel reactor (i.d. 9 mm) to remove the passivation layer by passing 60 ml/min of 10 vol.% H_2 in Ar while heating from 313 to 723 K at a rate of 2 K/min, and maintaining the final temperature for 1 h. The reactor was then cooled to 298 K in a flow of H_2. He flow at 30 ml/min was used to flush the catalyst for 30 min in order to achieve an adsorbate-free, reduced catalyst surface. After pre-treatment, 1 ml pulses of CO were injected into a flow of He (30 ml/min) and the CO uptake was measured using a TCD. CO pulses were repeatedly injected until the response from the detector showed no further CO uptake after consecutive injections and the total CO uptake, reported here in units of μmol/m^2, was obtained by dividing the uptake in μmol/g by the measured BET area. Assuming a 1:1 adsorption stoichiometry between CO and metal atoms, this value corresponds to the metal site density on the surface of the catalyst.

The catalyst Brønsted acid sites were titrated by *n*-propyl amine (*n*-PA) temperature-programmed desorption using the same reactor and TCD used for the CO chemisorption. A flow of He (30 ml/min) saturated at room temperature with *n*-propyl amine (Aldrich, 99.8%) passed through heated gas lines to the reactor containing about 1 g of catalyst that had been pre-treated as before. After a 2 h adsorption at 383 K, the reactor was flushed in pure He at a flow rate of 30 ml/min for 1 h to ensure that physically adsorbed *n*-PA was removed. The chemisorbed *n*-PA was then desorbed by ramping the reactor temperature from 383 to 973 K at a rate of 5 K/min and the TCD was used to quantify the amount of *n*-PA desorbed. The system was calibrated using three zeolite samples of known acidity.

2.3. Catalyst activity

The HDN of carbazole was carried out in a fixed bed reactor (i.d. = 9 mm) at 583 K and 3.0 MPa H_2. Approximately 1 g of the passivated catalyst ($d_p < 0.7$ mm) was activated at 723 K for 2 h in H_2 at a flow rate of 160 ml (STP)/min. The temperature was then cooled to the reaction temperature 583 K and the reaction was initiated using the appropriate feed flow conditions. Carbazole dissolved in xylene at a concentration of 3000 ppm was fed to the reactor using a Gilson Model 0154E metering pump. Prior to entering the reactor, the liquid was evaporated into a stream of flowing H_2. Gas and liquid flows and catalyst charged to the reactor were chosen to give a WHSV = 0.6 h^{-1}. The product was collected periodically and analyzed using a 3400 Varian Star Gas Chromatograph equipped with a flame ionization detector (FID). Component separation was achieved using a capillary column (CP-Sil 19 CB, 25 m length and 0.53 mm i.d.). Component identification was confirmed using the same column and a GC-MS (Agilent 6890/5973N).

3. Results

3.1. Catalyst properties

The TPR profiles of the bulk Ni_xMoP ($0.0 \leq x \leq 1.11$) precursors are shown in Fig. 1. The data show a clear trend of decreasing reduction temperature as the Ni content increases. For the $Ni_{1.1}MoP$ precursor, two reduction peaks are observed at about 840 and 995 K. The profile is similar to that reported for the bulk Ni_2P precursor [41] but with the peak temperatures about 50 K higher than for the Ni_2P precursor. The decreased reduction temperature with increased Ni content is indicative of a significant interaction between the Ni and the MoP that is discussed in more detail below.

The XRD patterns of the reduced catalysts, presented in Fig. 2, confirmed that metal phosphides had been prepared. MoP was the dominant phase, but as more Ni was added to the Ni_xMoP, the formation of a NiMoP phase was clearly evident. For the $Ni_{1.11}MoP$ catalyst the NiMoP phase was dominant. The XRD data were used to estimate the crystallite size (d_c) and the lattice parameters of the MoP phase, and the results are shown in Table 1. The crystallite size ranged from 16–22 nm for $0 \leq x \leq 1.11$ and as the Ni content of the Ni_xMoP catalyst increased, the MoP crystallite size also increased. The MoP lattice parameters were $a = 0.3241 \pm 0.009$ nm and $c = 0.3180 \pm 0.007$, in good agreement with the reported MoP lattice parameters of $a = 0.3223$ nm and $c = 0.3191$ [42]. Furthermore, there was no consistent reduction in the lattice parameter *c* as Ni content increased. In previous work, Ma et al. [39] prepared $Ni_{(2-x)}Mo_xP$ catalysts and showed the formation of solid solutions for a range of Ni/Mo ratios >1. In the present study, however, the (Ni + Mo) content of the Ni_xMoP catalysts increased as the Ni content increased and the XRD data show that with the preparation method and catalyst composition used herein, a catalyst with a mixture of NiMoP and MoP phases was produced.

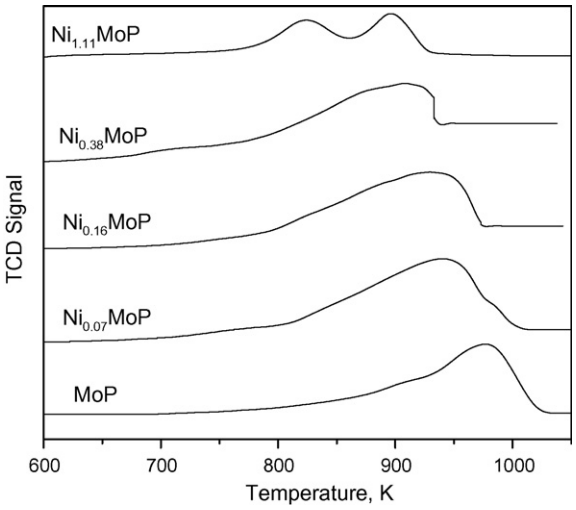

Fig. 1. TPR of calcined catalyst precursors (Ni_xMoP for $0.0 \leq x \leq 1.11$) measured in 10% H_2 in Ar at flow rate of 60 ml (STP)/min.

Table 2 reports the BET surface area, the CO chemisorption uptake and the *n*-PA uptake of the bulk Ni_xMoP catalysts. The BET surface area varied from 5.3 to 6.0 m^2/g for the Ni_xMoP

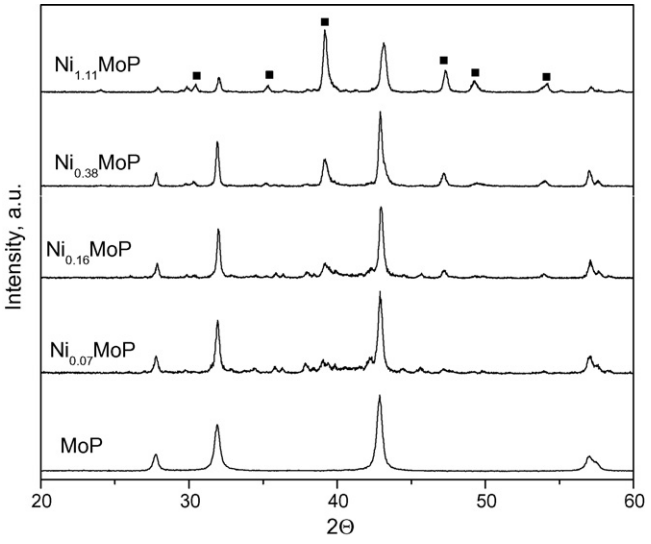

Fig. 2. X-ray diffractograms of all reduced Ni_xMoP for $0.0 \leq x \leq 1.11$. (■) NiMoP phase.

Table 1
Lattice parameters estimated from XRD data of reduced catalysts

Catalyst	Ni content (mol%)	Phases	MoP phase						
			2θ (°)				Lattice parameters (nm)		Crystallite size (nm)
			(1 0 0)	(1 0 1)	(1 1 0)	(1 1 1)	a	c	d_c (1 0 1)
MoP	0	MoP	31.93	42.89	57.16	64.93	0.3240	0.3196	16
$Ni_{0.07}MoP$	3	MoP	32.94	42.90	57.02	64.72	0.3255	0.3185	18
$Ni_{0.16}MoP$	7	MoP, NiMoP	31.98	42.96	57.08	64.68	0.3254	0.3182	21
$Ni_{0.38}MoP$	15	MoP, NiMoP	31.90	42.92	57.06	64.68	0.3256	0.3184	22
$Ni_{1.11}MoP$	34	MoP, NiMoP	32.04	43.16	57.12	64.72	0.3245	0.3170	22

($0 \leq x \leq 1.11$) catalysts and there is a minor increase in the surface area upon addition of Ni to MoP. The CO uptake and the *n*-PA uptake, reported per unit BET area of the catalysts, increased significantly with addition of Ni to the MoP. Furthermore, as the Ni content increased, the CO uptake increased whereas the *n*-PA uptake showed a maximum for the Ni_xMoP catalysts. Also note that the $Ni_{0.07}MoP$ catalyst had the lowest CO uptake and the highest *n*-PA uptake.

XPS was used to characterize the surfaces of the prepared catalysts and Fig. 3 shows the Ni 2p, Mo 3d and the P 2p spectra obtained. All the spectra showed oxidized Ni, Mo and P species because after synthesis, the catalysts were passivated using 2% O_2 in He to protect them from deep oxidation. The P $2p_{3/2}$ region showed a peak with a binding energy (BE) of 133.8 eV and another peak at 129.8 eV for all the prepared catalysts. Similar results have been reported earlier [26,43–45]. The peak at 133.8 eV is attributed to surface PO_4^{3-} species [43–45]. The lower BE peak at 129.8 eV is attributed to metal phosphides. The BE of the Ni 2p is consistent with the presence of metal phosphides and phosphates, corresponding to BEs of 853.7 and 857.3 eV, respectively. Similarly, Mo 3d BE at 228.2 and 232.2 eV indicates the formation of phosphide and phosphate species, respectively. The atom percentages of the prepared phosphides were also determined by XPS and the P/M atom ratios (where M is (Ni + Mo)) are reported in Table 2. The P/M atom ratios show that the $Ni_{0.07}MoP$ is slightly enriched in phosphorous (P/(Ni + Mo) ratio = 1.03) and increasing Ni content resulted in a decreased P/M ratio at the surface of the catalysts. Furthermore, the surface Ni/Mo ratio increased with increasing Ni content of the catalyst, although for the $Ni_{1.1}MoP$ catalyst, the surface Ni/Mo ratio was well below the nominal ratio of the bulk (Ni/Mo = 1.1), consistent with the presence of mixed MoP and NiMoP phases as observed by XRD.

Fig. 4 shows a correlation between the XPS and chemisorption data obtained on the metal phosphides of the present study. Assuming that the CO chemisorption titrates metal sites and the *n*-PA uptake titrates Brønsted acid sites, presumably associated with the surface phosphate species, the P/M atom ratio as determined by XPS should correlate with the *n*-PA to CO uptake ratio as determined by adsorption. The data plotted in Fig. 4 show a good correlation ($R^2 = 0.906$) and are consistent with a similar correlation determined for a series of Co_xNi_2P catalysts reported elsewhere [41].

3.2. Catalyst activity

Catalyst activity measurements were carried out using carbazole as the model reactant. The catalysts were passivated following synthesis and, therefore, prior to performing the activity measurements, the passivated catalysts were re-reduced in a H_2 flow at 723 K for 1 h. Catalyst conversion data were then measured and the conversions typically reached a steady value after about 8 h time-on-stream. The carbazole consumption rates reported in Table 3 are the time-averaged values over a period of at least 4 h that followed the initial 8 h stabilization period. In addition, for all the data reported herein, the carbon mole balance between the reactor feed and reactor effluent was >95%.

The data of Table 3 show that the carbazole conversion over the MoP catalyst was 55 mol%, whereas a significant increase occurred (86–90 mol%) for the Ni_xMoP catalysts ($0.07 \leq x \leq 1.11$). The carbazole consumption rates in terms of the specific rate, areal rate and TOF are also reported in Table 3. The areal rates are based on the measured BET surface area, whereas the specific rates are referred to the mass of catalyst used. The $Ni_{0.07}MoP$ catalyst had the highest

Table 2
Physiochemical properties of prepared metal phosphide

Catalyst	BET area (m^2/g)	Chemisorption		P/M[a]		Ni/Mo
		CO uptake (μmol/m^2)	*n*-PA uptake (μmol/m^2)	Nominal (atom ratio)	XPS (atom ratio)	XPS (atom ratio)
MoP	5.3	0.21	8	1.00	1.00	–
$Ni_{0.07}MoP$	6.0	0.83	40	0.93	1.03	0.07
$Ni_{0.16}MoP$	5.9	1.15	35	0.88	0.99	0.18
$Ni_{0.38}MoP$	5.9	1.26	29	0.78	0.93	0.27
$Ni_{1.11}MoP$	5.9	2.05	32	0.60	0.84	0.52

[a] M: total metals (Ni + Mo) and P: phosphorous.

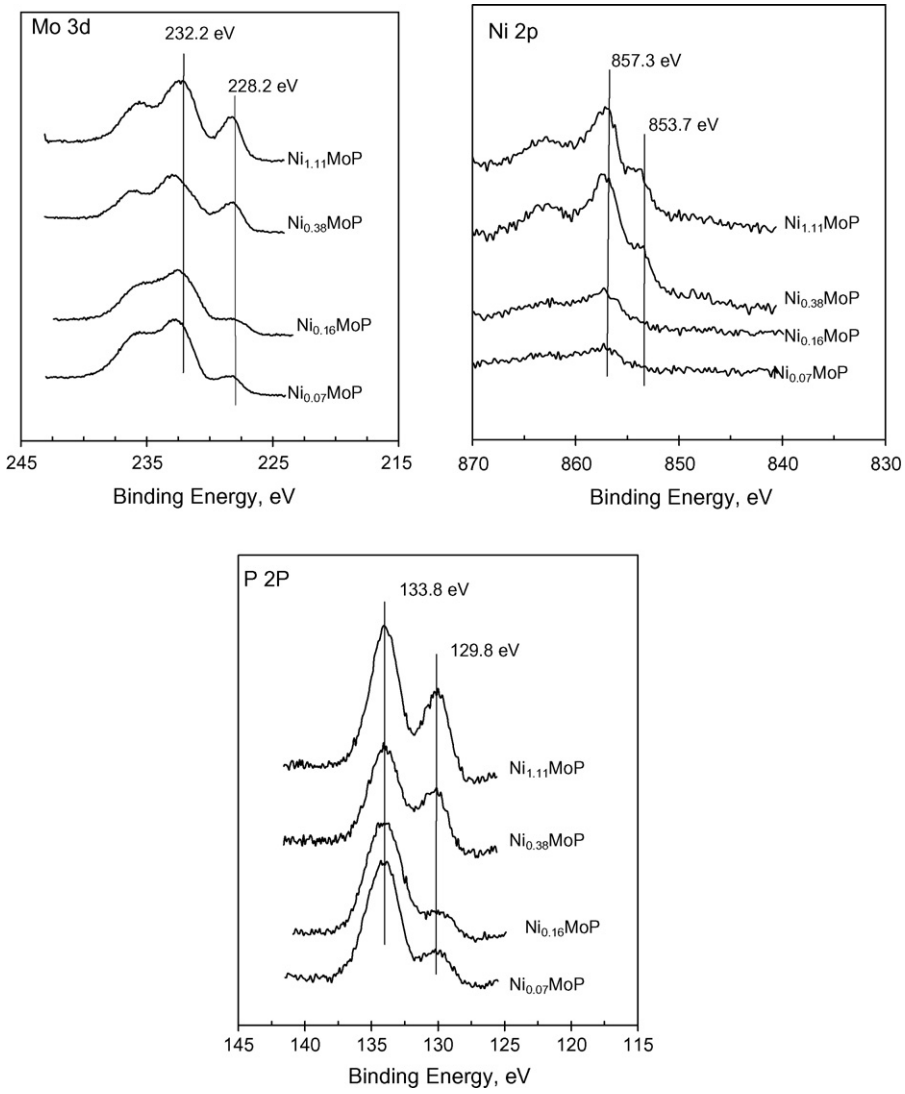

Fig. 3. XPS spectra of the Ni 2p, Mo 3d and P 2p of the prepared phosphides after reduction.

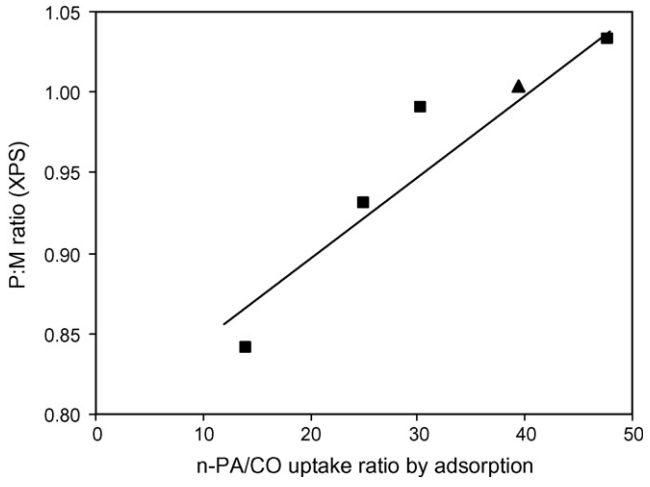

Fig. 4. Correlation of P/M ratio determined by XPS and *n*-PA:CO uptake ratio determined by adsorption for Ni_xMoP for $0.0 \leq x \leq 1.11$ (■) and MoP (▲).

specific and areal carbazole consumption rates, whereas the $Ni_{1.11}MoP$ catalyst had the lowest. However, in terms of TOF based on CO uptake, the MoP carbazole consumption is about three times greater than that of the $Ni_{0.07}MoP$ catalyst and this result is in agreement with previous studies that report the MoP catalyst activity is not promoted by addition of Ni [31].

The main reaction products of carbazole for all the catalysts were bicyclohexane (BCHX) and tetrahydrocarbazole (THCZ). Smaller quantities of cyclopentane cyclohexyl methane (CPCHX) were also identified by GC–MS. The direct hydrogenolysis product biphenyl was not observed. In addition, both the aromatic rings of the products were saturated and no products with partially hydrogenated aromatic rings were observed. There were also some cracked products identified by GC–MS and reported herein as a lumped group that had a carbon number < 12. The data of Table 3 show that the selectivity to BCHX of the Ni_xMoP catalyst was significantly greater than that obtained over MoP. Furthermore, for the Ni_xMoP catalysts, the BCHX selectivity decreased as the Ni

Table 3
Activities of bulk metal phosphides for the HDN of carbazole measured at 583 K and 3.0 MPa H_2

Catalyst	Total conversion (mol%)	Carbazole consumption rate			Selectivity				
		Specific ($\times 10^9$ mol g^{-1} s^{-1})	Areal ($\times 10^9$ mol m^{-2} s^{-1})	TOF ($\times 10^3$ s^{-1})	BCHX (mol%)	CPCHX (mol%)	THCZ (mol%)	Other products	
								BT (mol%)	AT (mol%)
MoP	54.5	5.61	1.37	6.59	20.5	4.3	26.0	30.9	16.0
$Ni_{0.07}MoP$	90.0	9.26	1.57	1.89	85.6	2.2	7.9	2.9	0.0
$Ni_{0.16}MoP$	89.6	9.22	1.56	1.36	77.8	0.7	17.0	0.5	0.4
$Ni_{0.38}MoP$	88.8	9.13	1.54	1.22	51.2	2.1	10.0	27.8	6.7
$Ni_{1.11}MoP$	85.8	8.83	1.49	0.73	40.4	3.3	17.5	34.9	2.4

BT: other products formed with carbon number < 12.
AT: other products formed with carbon number > 12.

content increased and the highest BCHX selectivity occurred for the $Ni_{0.07}MoP$ catalyst.

The carbazole conversion, BCHX selectivity and *n*-PA uptake are plotted as a function of the CO uptake in Fig. 5. As noted above, the data show a significant increase in *n*-PA uptake, BCHX selectivity and carbazole conversion with Ni addition to the MoP. However, as Ni content increased ($x > 0.07$ in Ni_xMoP) the *n*-PA uptake and BCHX selectivity decreased, with a small reduction in carbazole conversion.

4. Discussion

The data of Table 3 show that the activity of the MoP catalyst (1.4×10^{-9} mol m^{-2} s^{-1}) was slightly lower than the Ni_xMoP catalysts and the highest areal activity was obtained on the $Ni_{0.07}MoP$ catalyst with a value of 1.6×10^{-9} mol m^{-2} s^{-1} at 583 K and 3.0 MPa H_2. Areal rates of *o*-propylaniline HDN at 643 K and 3.1 MPa H_2 over metal phosphides have been reported by Stinner et al. [31]. Values of 312×10^{-9} mol m^{-2} s^{-1} and 55×10^{-9} mol m^{-2} s^{-1} were reported on bulk MoP and NiMoP, respectively. These activities are at least an order of magnitude higher than the values reported herein at 583 K and 3.0 MPa H_2 for carbazole HDN. Wang et al. [28] reported quinoline HDN

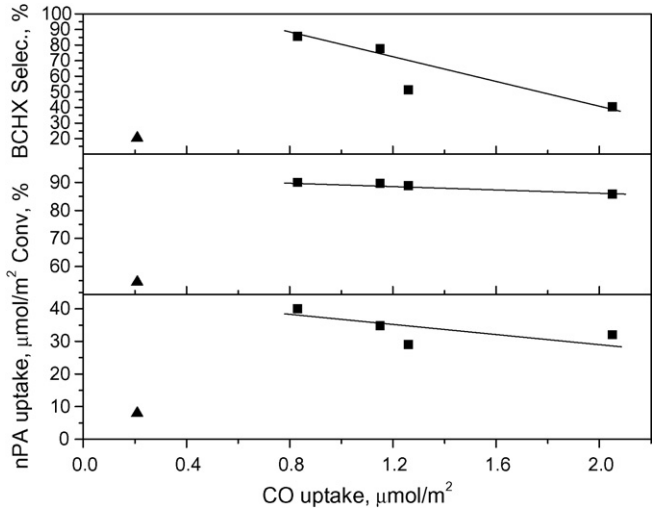

Fig. 5. Correlation of P/M ratio (determined by XPS) and *n*-PA/CO uptake ratio (determined by adsorption) with conversion and BCHX selectivity of Ni_xMoP (■) $0.0 \leq x \leq 1.11$ and MoP (▲) catalysts.

TOF data for supported CoP (1.2×10^{-3} s^{-1}) and supported Ni_2P (0.60×10^{-3} s^{-1}) at 643 K and 3.1 MPa in the presence of dibenzothiophene. The relatively low activity of quinoline at this temperature was attributed in part to the inhibiting effects of the sulfur compound. Carbazole is a non-basic, five-membered N-heterocycle in which the extra pair of electrons of N are involved in π electron-cloud bonding and therefore are not available for interaction with the catalyst surface [47]. Hence, carbazole has a low reactivity that makes it difficult to remove the N heteroatom and the data reported herein are consistent with this observation. The data of Table 3 also show that the bulk MoP had the highest TOF among the catalysts tested. On bulk MoP, a TOF of 6.6×10^{-3} s^{-1} was obtained after an initial 8 h of reaction at 583 K and 3.0 MPa. The activity compares favorably to that reported for Mo_2N with the same reactant. Nagai et al. [46] reported a TOF for carbazole HDN of 29×10^{-3} s^{-1} over nitrided 12.5 wt% Mo/Al_2O_3, measured in a fixed bed microreactor at 573 K and 10.1 MPa. However, the Mo_2N catalyst TOF was determined after 30 min time-on-stream and the activity decreased by a factor of about two within 2 h time-on-stream [46].

The catalyst activity and selectivity during carbazole HDN can be related to the catalyst properties. The XPS and adsorption data of Fig. 4 suggest that metal sites are associated with CO adsorption and acid sites are associated with P, and these observations are consistent with similar data reported for Co_xNi_2P catalysts [41]. The source of the Brønsted acidity on the bulk phosphide is likely a consequence of the pretreatment of the catalysts before reaction with H_2 at 723 K, that leads to formation of water with the most reactive passivated oxygen. The water may react with surface phosphate to produce the $H_xPO_4^{(x-3)}$ species responsible for the Brønsted acidity. The Ni_xMoP catalysts all had higher metal and acid site densities than the MoP catalysts. Although a slight P enrichment of the surface occurred for $Ni_{0.07}MoP$ compared to MoP, the P content decreased as more Ni was added to the Ni_xMoP catalysts. The data of Fig. 5 show that the acid site density decrease associated with the Ni content of Ni_xMoP is relatively small when compared to the MoP data. The selectivity for BCHX among the metal phosphides was highest on the $Ni_{0.07}MoP$ catalyst. However, as the Ni content of the Ni_xMoP catalysts increased, the selectivity to BCHX decreased in favor of lighter products. In all cases, however, the MoP had lower BCHX selectivity than

the Ni_xMoP catalysts. A significant increase in conversion and BCHX selectivity is observed when comparing MoP to the Ni_xMoP catalysts. However, for the series of Ni_xMoP catalysts, the conversion is relatively constant as CO uptake increases, whereas selectivity to BCHX decreases. Indeed the trend in BCHX selectivity follows the trend in *n*-PA site density as CO uptake increases. More significantly, however, the increased CO uptake corresponds to an increase in the surface Ni/Mo ratio, determined by XPS. The uptake of CO by Ni_2P is known to be less than that of MoP [41] and Sun et al. [50] have reported a decrease in CO uptake with increased Ni content for a series of Ni–Mo–P/SiO_2 supported catalysts. Furthermore, they report that CO infra red spectra on these catalysts did not show characteristic adsorption bands for CO on Mo, from which they concluded that much of the Ni was exposed on the surface and that the surface was therefore similar to Ni_2P/SiO_2. In the present study, however, the CO uptake increased with Ni content as did the M/P and Ni/Mo surface ratio as determined by XPS (Table 2). Furthermore, the XRD data showed that a new phase, NiMoP was formed at high Ni content. A possible explanation for these differences is that in the bulk catalyst of the present study, a well dispersed NiMoP phase is generated and this phase is mostly responsible for the increased CO uptake.

Fig. 6 shows the proposed reaction scheme for the HDN of carbazole on nitrided Mo/Al_2O_3 catalyst [46]. The authors attributed BCHX formation to C–N hydrogenolysis of the perhydrocarbazole, and the cyclohexylbenzene and cyclohexylcyclohexene to C–N hydrogenolysis of the hexahydrocarbazole and decahydrocarbazole, respectively. Clark et al. [48] have noted that acid sites alone do not lead to active hydroprocessing catalysts. According to these authors, C–N bond cleavage on MoP catalysts is dominated by a Hoffman type elimination reaction, in which both the α- and β-carbon atoms need to be saturated to allow the C–N hydrogenolysis reaction to take place. Hence the activity of catalysts towards unsaturated hydrocarbons is limited by the hydrogenation ability of the catalyst. The HDN of heterocyclic compounds proceeds by hydrogenation of the aromatic ring and then subsequent hydrogenolysis of the C–N bond [35]. Hydrogenation and hydrogenolysis occur on two types of catalytic sites that are responsible for the direct $C(sp^2)$–N bond hydrogenolysis and hydrogenation and $C(sp^3)$–N bond cleavage during the HDN reaction [38]. On the MoP catalyst, moderate activity is obtained with low selectivity to the BCHX and higher selectivity to THCZ. Addition of Ni to MoP yields increased metal sites (based on CO uptake and XPS data) that also increased catalyst hydrogenation activity. Similar effects of Ni have been observed by Jian and Prins [38], who reported that MoP was a better catalyst for the direct C–N bond hydrogenolysis but on addition of Ni, the hydrogenation activity increased significantly. Similarly, Wada et al. [49] reported that on introduction of the noble metals to Ni/Y-zeolite, higher hydrogenation activity was obtained.

An increased hydrogenation capability of the Ni_xMoP catalyst yielded higher selectivity to BCHX and lower selectivity to THCZ, compared to MoP. The higher BCHX selectivity is a consequence of the formation of more $C(sp^3)$–N

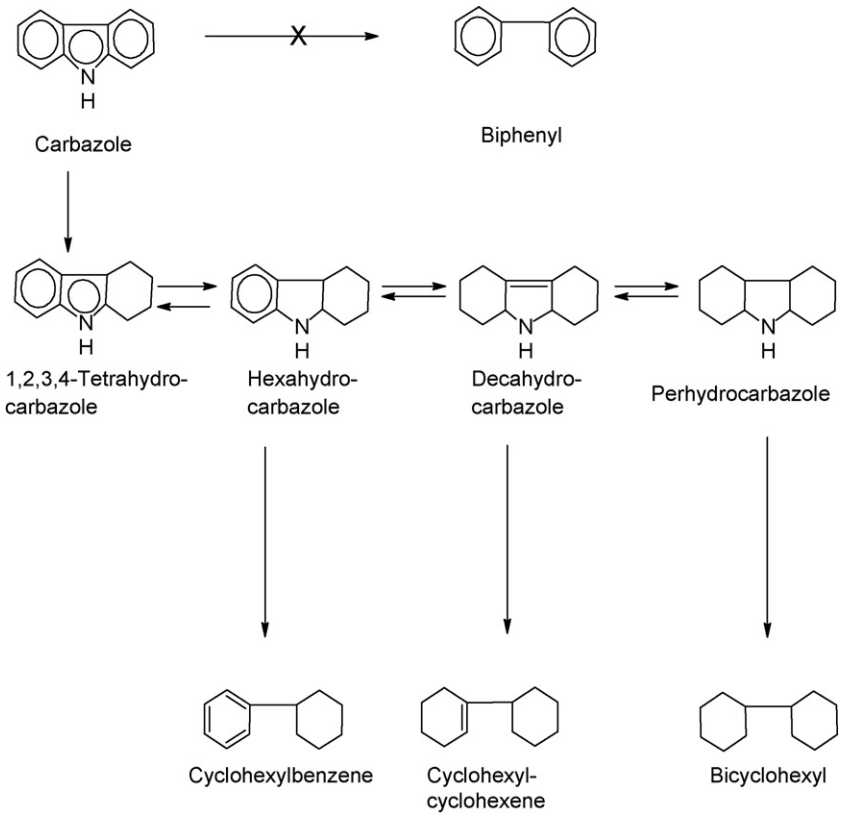

Fig. 6. General reaction scheme of HDN of carbazole [46].

bonds that result from increased hydrogenation by Ni_xMoP catalysts compared to MoP, and these bonds are readily cleaved. The data of Fig. 5 also suggest that the bond cleavage is related to the acid sites of the catalysts since for the Ni_xMoP series, as the metal site density increases, the acid site density decreases as does the selectivity to BCHX. The products from carbazole HDN included small amounts of CPCHX, likely produced as a result of ring opening or isomerization due to Brønsted acidity. After hydrogenation of the aromatic rings and the C–N hydrogenolysis, the resulting molecule may undergo a C–C bond cleavage and isomerization to form a five-member carbon ring while leaving one of the six-member saturated aromatic rings intact to produce the CPCHX product.

5. Conclusions

In the present study, Ni_xMoP had a lower TOF for the HDN of carbazole compared with MoP. However, the selectivity to BCHX was greater on the Ni_xMoP catalysts compared to MoP, and the $Ni_{0.07}MoP$ had the highest BCHX selectivity and highest TOF among the Ni_xMoP series. The improved selectivity is attributed to enhanced hydrogenation in the presence of the Ni_xMoP catalyst and increased C–N bond cleavage, attributed to the acidity of the catalyst.

Acknowledgements

Financial support from the Natural Sciences and Engineering Research Council of Canada is gratefully acknowledged. IA thanks the Canadian Commonwealth Scholarship and Fellowship Program and the Government of Ghana for financial aid.

References

[1] J.N. Heresnope, J.E. Morris, British Patent 701 (1957) 217.
[2] J.N. Housam, R. Lester, British Patent 807 (1959) 583.
[3] J.A.R. van Veen, H.A. Colijn, P. Hendriks, A.J. vanWelsenes, Fuel Process. Technol. 35 (1993) 137.
[4] C.W. Fitz, H.F. Rase, Ind. Eng. Chem. Prod. Res. Dev. 22 (1983) 40.
[5] R.E. Tischer, N.K. Narain, G.J. Stiegel, D.L. Cillo, Ind. Eng. Chem. Res. 26 (1991) 412.
[6] S. Eijsbouts, J.N.M. van Gestel, J.A.R. van Veen, V.H.J. de Beer, R. Prins, J. Catal. 131 (1991) 412.
[7] G.A. Mickelson, US Patents 3 749 633, 3 749 664, 3 755 148, 3 755 150 & 3 755 196, 1973.
[8] M. Jian, F. Kapteijn, R. Prins, J. Catal. 168 (1997) 491.
[9] H. Kraus, R. Prins, J. Catal. 170 (1997) 20.
[10] R. Iwammoto, J. Grimbolt, Stud. Surf. Sci. Catal. 127 (1999) 169.
[11] M. Lewandoski, Z. Sarbak, Fuel 79 (2000) 487.
[12] M. Jian, R. Cerda, R. Prins, Bull. Soc. Chim. Belg. 104 (1995) 225.
[13] W.R.A.M. Robinson, J.N.M. Van Gestel, T.I. Koranyi, S. Eijsbouts, A.M. Van der Kraan, J.A.R. Van Veen, V.H.J. De Beer, J. Catal. 161 (1996) 539.
[14] P.J. Mangnus, A.D. van Langeveld, V.H.J. de Beer, J. Catal. 161 (1996) 539.
[15] R. Prins, P. Gerhard, Th. Werber, CHIMIA 10 (2001) 55.
[16] X. Tiancum, W. Hariato, D. Jianwen, K.S. Coleman, M.L.H. Green, J. Catal. 211 (2002) 183.
[17] L. Senzi, L. Jae, J. Catal. 173 (1998) 134.
[18] C.W. Colling, L.T. Thompson, J. Catal. 146 (1994) 193.
[19] S. Krysztof, H.S. Kim, C. Sayag, D. Brodzki, G. Djega-Mariadassou, Catal. Lett. 53 (1998) 59.
[20] S. Ramanathan, C.C. Yu, S.T. Oyama, J. Catal. 173 (1998) 10.
[21] R. Prins, G. Pirngruber, T. Weber, Chimia 55 (2001) 791.
[22] W. Li, B. Dhandapani, S.T. Oyama, Chem. Lett. 207 (1998) 207.
[23] S.T. Oyama, P. Clark, L.S. Teixeira da Siva, E.J. Lede, F.G. Requejo, J. Phys. Chem. 105 (2001) 4961.
[24] P. Clark, W. Li, S.T. Oyama, J. Catal. 200 (2001) 140.
[25] C. Stinner, R. Prins, Th. Weber, J. Catal. 191 (2000) 434.
[26] D.C. Phillips, S.J. Sawhill, R. Self, M.E. Bussel, J. Catal. 20 (2002) 266.
[27] S.T. Oyama, J. Catal. 216 (2003) 343.
[28] X. Wang, P. Clark, S.T. Oyama, J. Catal. 208 (2002) 321.
[29] S.T. Oyama, X.T. Wang, F.G. Requejo, T. Sato, Y. Yoshimura, J. Catal. 209 (2002) 1.
[30] V. Zuzaniuk, R. Prins, J. Catal. 219 (2003) 85.
[31] C. Stinner, R. Prins, Th. Weber, J. Catal. 202 (2001) 187.
[32] S.J. Sawhill, D.C. Phillips, M.E. Bussell, J. Catal. 215 (2003) 208.
[33] P.A. Clark, S.T. Oyama, J. Catal. 218 (2003) 78.
[34] A. Stanislaus, B.H. Coopet, Catal. Rev. Sci. Eng. 36 (1994) 75.
[35] R. Prins, M. Jian, M. Flechsenhar, Polyhedron 16 (18) (1997) 3235.
[36] R. Prins, M. Egorova, A. Röthlisberger, Y. Zhao, N. Sivasankar, P. Kukula, Catal. Today 111 (2006) 84.
[37] K.J. Weller, P.A. Fox, S.D. Gray, D.E. Wigley, Polyhedron 11 (18) (1997) 3139.
[38] M. Jian, R. Prins, Catal. Today 30 (1996) 127.
[39] D. Ma, T. Xiao, S. Xie, W. Zhou, S.L. Gonzalez-Cortes, M.L.H. Green, Chem. Mater. 16 (2004) 2697.
[40] S.K. Maity, J. Ancheyta, M.S. Rana, P. Rayo, Catal. Today 100 (2005) 42.
[41] I.I. Abu, K.J. Smith, J. Catal. 241 (2006) 356.
[42] S. Harris, R.R. Chianelli, J. Catal. 98 (1986) 17.
[43] Y. Okamoto, Y. Niha, T. Imanaka, S. Teranishi, J. Catal. 64 (1980) 397.
[44] Y. Okamoto, K. Fukino, T. Imanak, S. Teranishi, J. Catal. 74 (1982) 17.
[45] Y. Okamoto, K. Fukino, T. Imanak, S. Teranishi, J. Catal. 74 (1982) 173.
[46] M. Nagai, Y. Goto, A. Irisawa, S. Omi, J. Catal. 191 (2000) 128.
[47] M.V. Landau, Catal. Today 36 (1997) 393–429.
[48] P. Clark, X. Wang, P. Deck, S.T. Oyama, J. Catal. 210 (2002) 116.
[49] T. Wada, K. Kareda, S. Murata, M. Nomura, Catal. Today 31 (1996) 113.
[50] F. Sun, W. Wu, Z. Wu, J. Guo, Z. Wei, Y. Yang, Z. Jiang, F. Tian, C. Li, J. Catal. 228 (2004) 298.